

pH Switchable Nanoplatfom for In Vivo Persistent Luminescence Imaging and Precise Photothermal Therapy of Bacterial Infection

Li-Xia Yan, Li-Jian Chen, Xu Zhao, and Xiu-Ping Yan*

Photothermal therapy (PTT) is one of the most promising approaches to combat multidrug-resistant bacteria with less potential to induce resistance and systemic toxicity. However, uncontrollable distribution of photothermal agents leads to lethal temperatures for normal cells, and failure to offer timely and effective antibacterial stewardship. A pH switchable nanoplatfom for persistent luminescence imaging-guided precise PTT to selectively destroy only pathological cells while protecting nearby normal cells in bacterial infected microenvironment is shown. The PLNP@PANI-GCS is fabricated by grafting polyaniline (PANI) and glycol chitosan (GCS) onto the surface of persistent luminescence nanoparticles (PLNPs). It takes advantage of the long persistent luminescence of PLNPs to realize autofluorescence-free imaging, the pH-dependent light–heat conversion property of PANI to get a stronger photothermal effect at pH 6.5 than pH 7.4, and the pH environment responsive surface charge transition of GCS. Consequently, PLNP@PANI-GCS enables effective response to bacterial-infected acid region and electrostatic bonding to bacteria in vivo, ensuring the spatial accuracy of near-infrared light irradiation and specific heating directly to bacteria. In vivo imaging-guided PTT to bacterial infection abscess shows effective treatment. PLNP@PANI-GCS has great potential in treating multidrug-resistant bacterial infection with low possibility of developing microbial drug resistance and little harm to normal cells.

1. Introduction

Pathogenic bacterial infection, one of the most serious risks in medicine, food, and other fields, causes about nearly one-third of death globally and poses a serious threat to human health.^[1] Antibiotics have been widely used for bacterial infection as a most accepted treatment. However, the inappropriate use, especially overuse of antibiotics has caused the emergence of multidrug-resistant (MDR) bacterial strains such as methicillin-resistant *Staphylococcus aureus* (MRSA), inducing skin and soft tissue intractable infection, and leading to a high mortality. MDR bacterial infection may cause 10 million annual deaths by 2050.^[2] Since MDR bacteria can rapidly develop antibiotic resistance, alternative therapeutic strategies with low possibility for the development of microbial drug resistance is urgently needed.^[3]


Photothermal therapy (PTT) which kills bacteria by physical heat is one of the most promising novel approaches, because of its preferable ability to combat MDR bacteria with less potential to induce resistance and systemic toxicity. Particularly, PTT based on near-infrared (NIR) light irradiation has been widely developed due

to the improved tissue penetration of NIR light.^[4] Considerable efforts have focused on NIR light-triggered inorganic materials, including gold nanoparticles,^[5] transitional metal dichalcogenide,^[6] carbon nanomaterials,^[7] palladium nanosheets,^[8] and others.^[9] However, the lack of biodegradability and the potential for long-term toxicity limit their clinical application. Unlike inorganic materials, organic PTT agents can be designed and fine-tuned via dedicated synthesis for applications.^[10] Organic nanoparticles such as NIR absorbing conjugated polymers,^[11] cyanines,^[12] and porphyrins^[13] have been widely explored. Recently, nontoxic organic polymers such as polyaniline (PANI) and polypyrrole have been shown as promising photothermal agents for cancer ablation in vitro and in vivo.^[14] Among these popular polymeric photothermal agents, PANI is the most potential one due to its good conductivity, mechanical flexibility, photostability, biodegradability, and high photothermal conversion efficiency.^[15] Furthermore, PANI has been successfully used as electroactive materials in cellular proliferation study

L.-X. Yan, Dr. L.-J. Chen, Dr. X. Zhao, Prof. X.-P. Yan
State Key Laboratory of Food Science and Technology
International Joint Laboratory on Food Safety
Jiangnan University
Wuxi 214122, China
E-mail: xpyan@jiangnan.edu.cn

L.-X. Yan, Dr. L.-J. Chen, Dr. X. Zhao, Prof. X.-P. Yan
Institute of Analytical Food Safety
School of Food Science and Technology
Jiangnan University
Wuxi 214122, China

Prof. X.-P. Yan
Key Laboratory of Synthetic and Biological Colloids
Jiangnan University
Ministry of Education
Wuxi 214122, China

 The ORCID identification number(s) for the author(s) of this article can be found under <https://doi.org/10.1002/adfm.201909042>.

DOI: 10.1002/adfm.201909042

due to its noncytotoxicity.^[16] In particular, PANI can improve its photothermal conversion efficiency under acidic conditions, which is favorable for selective destroy of only pathological cells with simultaneous protection of nearby normal cells.^[14a,15b]

However, the therapy-only functional approaches are unable to offer timely and effective antibacterial stewardship. To facilitate precise therapy, a visualized theranostic platform is needed for accurate diagnosis, infection lesion imaging, and real-time monitoring of treatment in a single nanosystem. Persistent luminescence nanoparticles (PLNPs) are promising optical materials which show long-lasting luminescence after stopping excitation. This unique optical property allows autofluorescence-free persistent luminescence imaging without the need for in situ excitation.^[17] Moreover, Cr³⁺-doped NIR-emitting PLNPs have additional advantages of deep penetration with super-long afterglow, and renewability with tissue-penetrating red LED light instead of UV light, making PLNP-based imaging no longer limited by afterglow time.^[18] Therefore, Cr³⁺-doped PLNPs are not only suitable for autofluorescence-free bioimaging and long-term in vivo tracing, but also ideal materials to build visualized theranostic nanoplatfroms.

Herein, we report the design and fabrication of PANI and glycol chitosan (GCS) functionalized pH switchable nanoplatfrom for in vivo persistent luminescent bacterial infection imaging and precise photothermal therapy. NIR-emitting PLNP (Zn_{1.2}Ga_{1.6}Ge_{0.2}O₄:Cr³⁺) is used as the core for its renewable NIR-persistent luminescence by 650 nm LED light, while PANI is employed as the shell for the high photothermal conversion efficiency under acidic condition. The core-shell nanomaterials PLNP@PANI is further functionalized with GCS to obtain pH-responsive nanoplatfrom PLNP@PANI-GCS for targeting acidic abscesses microenvironment and improving the biocompatibility of hydrophobic PANI shell. GCS is a water-soluble biopolymer with pH-dependent charge that has been widely studied in various biomedical applications.^[19] The obtained PLNP@PANI-GCS turns to positive charge, specifically aggregates in the acidic bacterial-infection abscesses via strong electrostatic interaction with negatively charged bacteria cell walls, gives activated photothermal effect in abscesses acidic microenvironment. Moreover, PLNP@PANI-GCS shows negligible side effect to normal cells as it becomes slightly negatively charged at normal physiological pH and exhibits poor affinity to neighboring normal cells as well as poor photothermal effect in normal physiological environment. This multifunctional nanoplatfrom provides a targeted autofluorescence-free luminescence imaging-guided precise and visualized PTT to the treatment of bacterial infection with an enhanced photothermal effect to bacteria but little harm to normal cells.

2. Results and Discussion

2.1. Fabrication and Characterization of PLNP@PANI-GCS

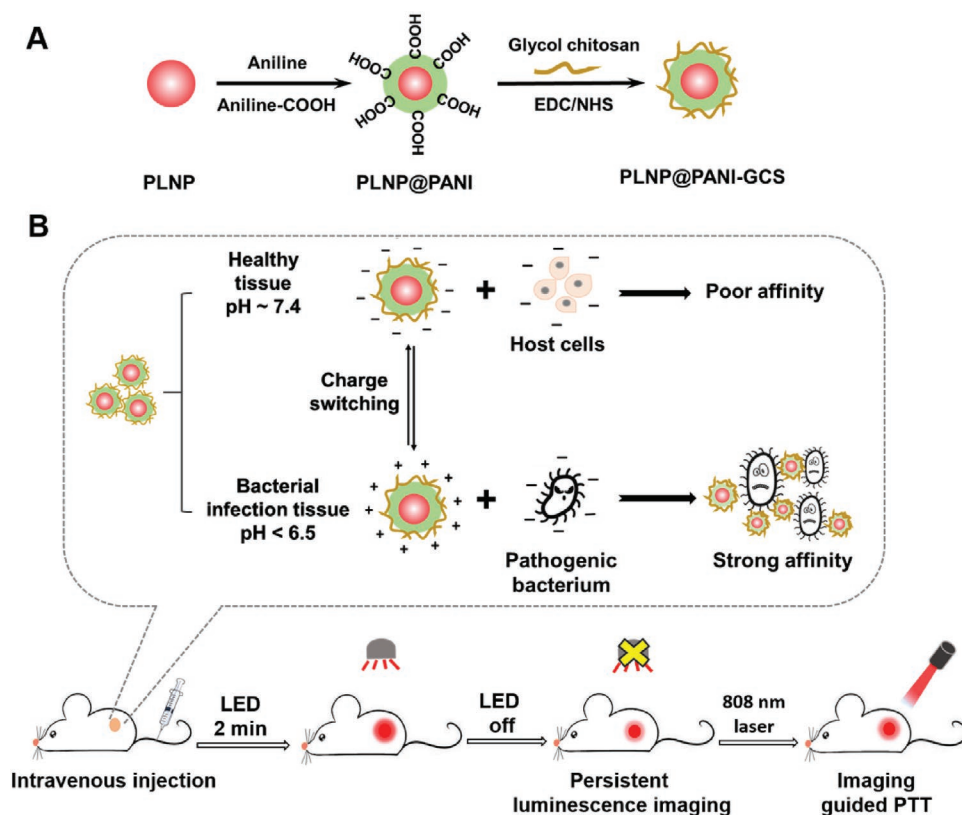
The design and preparation of our multifunctional nanoplatfrom PLNP@PANI-GCS is illustrated in **Scheme 1A**. To achieve autofluorescence-free bioimaging, we synthesized Zn_{1.2}Ga_{1.6}Ge_{0.2}O₄:Cr³⁺ PLNPs as the core of the nanoplatfrom due to its long-lasting

and red light reversible reactivated NIR-persistent luminescence.^[20] The encapsulation of PLNPs by PANI was achieved via the oxidative polymerization of aniline and aniline-COOH. PLNP@PANI was then functionalized with GCS by means of amidation reaction to obtain charge conversion capability and to improve biocompatibility. The utilization of PLNP@PANI-GCS for targeting and specific persistent luminescence imaging-guided photothermal therapy of bacterial-infected abscesses is shown in **Scheme 1B**. The PLNP@PANI-GCS intravenously injected into mice would become positively charged in the acidic bacterial-infection abscesses, and specifically aggregate in this region via strong electrostatic interaction with negatively charged bacteria. However, PLNP@PANI-GCS would become slightly negatively charged at normal physiological pH and exhibit poor affinity to neighbouring negatively charged normal cells. In addition, the aggregated PLNP@PANI-GCS in acid bacterial infection region would give an enhanced photothermal effect than in normal physiological pH region because of the higher photothermal conversion efficiency of PANI under acidic condition. Thus, PLNP@PANI-GCS enables targeted autofluorescence-free luminescence imaging-guided precise and visualized PTT to bacterial infection.

The as-synthesized Zn_{1.2}Ga_{1.6}Ge_{0.2}O₄:Cr³⁺ core gave an average size of 16.3 ± 3.5 nm (based on 155 randomly selected nanoparticles) (**Figure S1A, B**, Supporting Information) with a pure spinel phase of Zn₂GeO₄ (JCPDS 25-1018) and ZnGa₂O₄ (JCPDS 38-1240) (**Figure S1C**, Supporting Information). The solid PLNPs gave a NIR emission peak at 700 nm after 254 nm UV light excitation (**Figure S1D**, Supporting Information). The persistent luminescence signal of PLNPs could be easily captured on an IVIS imaging system (**Figure S2A**, Supporting Information). PLNPs in aqueous solution (1 mg mL⁻¹) exhibited similar optical properties (**Figure S2B**, Supporting Information) with long-lasting afterglow (**Figure S2C**, Supporting Information). Importantly, the NIR luminescence of PLNPs could be reactivated with minimal loss under red LED light excitation (**Figure S2D**, Supporting Information), making it suitable for long-term autofluorescence-free in vivo and real-time imaging.

The encapsulation of PLNPs by PANI was achieved via the oxidative polymerization of aniline and aniline-COOH in sodium dodecyl sulfate (SDS) aqueous solution. The aniline molecules were adsorbed onto the surface of PLNPs due to the electrostatic force, then the polymerization occurred to form core-shell PLNP@PANI with the -COOH groups on the surface upon the addition of ammonium persulfate solution (APS). SDS molecules embed its hydrophobic tail in the aniline layer, while the negative sulfate groups stabilized the nanoparticles.^[2a] PLNP@PANI was then functionalized with GCS to obtain charge conversion capability and to improve biocompatibility. Subsequent amidation reaction between PLNP@PANI and GCS gave PLNP@PANI-GCS.

The obtained PLNP@PANI and PLNP@PANI-GCS showed a discernible core-shell nanostructure with the PANI shell thickness of about 2 nm and a total 5 nm thick layer coating of final PLNP@PANI-GCS (**Figure 1A**; **Figure S3**, Supporting Information). The elements Zn, Ga, Ge, and O were mainly distributed in the core, and the element N in the whole nanostructures, suggesting the success synthesis of PANI shell on PLNP. Further GCS modification made the obvious C element



Scheme 1. A) Schematic for the preparation of PLNP@PANI-GCS. B) Illustration of PLNP@PANI-GCS for persistent luminescence imaging-guided photothermal therapy of bacterial infection.

mapping on PLNP@PANI-GCS (Figure S3, Supporting Information). TGA curve showed that the weight loss percentage of PANI and GCS was 3.9% and 17.0%, respectively (Figure 1B). The grafted amount of PANI and GCS on PLNP was 0.01 and 0.049 mg per mg of PLNP, respectively. PANI shell functionalization increased the zeta potential from -30.9 mV (PLNPs) to -25.4 mV (PLNP@PANI), while subsequent GCS modification increased the zeta potential to 19 mV (PLNP@PANI-GCS) at pH 6.5 due to the charge conversion capacity of GCS (Figure 1C). The hydrodynamic size of the PLNPs increased from 60.9 nm (PDI 0.260) to the final 293.5 nm (PDI 0.163), which also reveals the successful surface modification of PLNP (Figure 1D). PLNP@PANI and PLNP@PANI-GCS gave similar persistent luminescence properties of PLNP with a NIR-persistent luminescence peak at 700 nm after 254 nm UV light excitation, but a little lower intensity than PLNP due to the modification of PANI (Figure S4, Supporting Information). The persistent luminescence of PLNP@PANI and PLNP@PANI-GCS can also be reactivated with red LED light (Figure S4B, Supporting Information). The PLNP@PANI-GCS exhibited no significant difference in persistent luminescence performance at pH 6.5 and 7.4 (Figure S4B, Supporting Information). The persistent luminescence signal of PLNP@PANI-GCS captured on an IVIS imaging system further gave consistent results, the PLNP@PANI-GCS maintained long persistent luminescence properties after UV excitation and could be easily reactivated with a red LED light (Figure 1E), indicating the potential of PLNP@PANI-GCS for in vivo imaging applications.

The surface modification of PLNPs was further confirmed by Fourier transform infrared (FT-IR) spectroscopy (Figure 1F). PLNP@PANI gave strong absorption bands at 1580 and 1495 cm^{-1} for C=C stretching vibration of the quinoid and benzenoid rings, respectively, 1299 and 1242 cm^{-1} for C-N stretching of the benzenoid rings and C=N stretching of the quinoid rings, respectively.^[19b,21] Besides, the absorption band of C-O stretching vibration at 1130 cm^{-1} in combination with the carboxylate asymmetric stretching vibration near 1600 cm^{-1} (overshadowed by the stronger C=N band of PANI at 1580 cm^{-1}) indicates the existence of $-\text{COOH}$ groups on the PLNP@PANI. After GCS functionalization, the stretching vibration of $-\text{CO}-\text{NH}-$ at 1642 cm^{-1} appeared. The asymmetric and symmetric C-H stretching bands at 2975 , 2927 , and 2856 cm^{-1} and the C-O stretching vibration of GCS at 1050 cm^{-1} , as well as the N-H stretching bands at 3420 cm^{-1} confirm the successful GCS modification. Time-dependent analysis of the hydrodynamic diameter, phosphorescence, UV-vis-NIR, and FT-IR spectra shows that PLNP@PANI-GCS is relatively stable at pH 6.5 and 7.4 over 240 h (Figures S5-S7, Supporting Information).

GCS modification on PLNP@PANI is the key to realize charge conversion in acid environment. So, we examined the zeta potentials of the PLNP@PANI-GCS at different pH with various modified ratios of GCS (Figure 2A). The results reveal that the PLNP@PANI-GCS was converted from slight negative charge at pH 7.4 to positive charge as pH decreased. The zeta potential of PLNP@PANI-GCS changed from -4.7 mV (pH 7.4) to 19.0 mV (pH 6.5) at the feeding weight ratio of 1:10 PLNP@PANI to

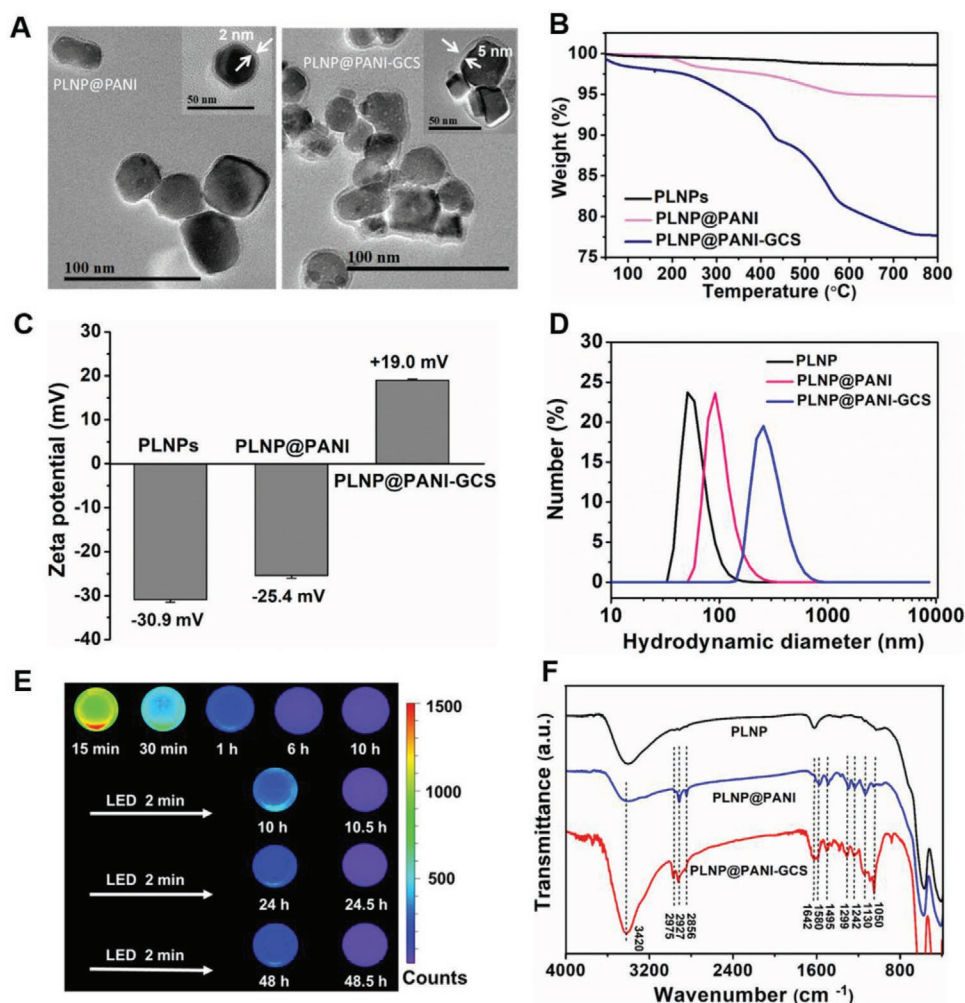


Figure 1. Characterization of surface functionalized persistent luminescence nanoparticles (PLNPs): A) TEM image of PLNP@PANI and PLNP@PANI-GCS. B) TGA curves of PLNP, PLNP@PANI, and PLNP@PANI-GCS. C) Zeta potential of PLNP, PLNP@PANI, and PLNP@PANI-GCS (pH 6.5). D) Hydrodynamic diameters of PLNP, PLNP@PANI, and PLNP@PANI-GCS. E) Near-infrared (NIR) persistent luminescence images of PLNP@PANI-GCS aqueous solution (1 mL, 1 mg mL⁻¹ as PLNPs). The aqueous sample was prior illuminated with a UV lamp for 5 min and nature decay of luminescence was recorded on a CCD camera up to 10 h, and the sample was reactivated at 10, 24, and 48 h with a LED for 2 min, respectively. F) FT-IR spectra of PLNP, PLNP@PANI, and PLNP@PANI-GCS.

GCS. So, we choose the PLNP@PANI-GCS synthesized in this 1:10 weight ratio for all the experiments. However, PLNP@PANI was negatively charged even at pH 6.0 without GCS (1:0) in reaction system, implying that the effective modification of GCS endowed PLNP@PANI-GCS pH-sensitive charge conversion capability. As the number of protonated-free amine groups on their GCS backbones increases under the acidic environment,^[22] the surface charge of PLNP@PANI-GCS is convertible in a local pH-dependent manner.

2.2. Photothermal Properties of PLNP@PANI-GCS

Effective PTT agents should respond quickly and strongly to light excitation in a targeted area of subcutaneous tissue. 808 nm NIR laser is considered as one of the best suitable light sources for PTT owing to its low absorbance by tissue, blood, and water, and high penetration to the skin (up to a

depth of 10 mm).^[23] So, we examined the hyperthermic potential of PLNP@PANI-GCS under 808 nm NIR laser irradiation. Various concentrations of PLNP@PANI-GCS in phosphate-buffered saline (PBS, pH 6.5) were exposed to an 808 nm laser (1.5 W cm⁻²) with pure PBS solution as control, and the temperature was real-time recorded by infrared camera (Figure 2B; Figure S8A, Supporting Information). The PBS solution exhibited slight change in temperature from 22.8 to 24.4 °C even after 8-min irradiation with 808 nm laser (Figure 2B). In contrast, the temperature of PLNP@PANI-GCS solution increased rapidly upon 808 nm laser irradiation. 808 nm laser irradiation for 8 min made the temperature of the PLNP@PANI-GCS solutions with concentration of 1.0 and 1.5 mg mL⁻¹ (as PLNPs) increased up to 61.0 and 66.3 °C, respectively (Figure 2B). Since thermal ablation of most microbes occurs at temperature over 50 °C, PLNP@PANI-GCS in concentration of 1.0 mg mL⁻¹ in combination with 8-min 808 nm laser irradiation (1.5 W cm⁻²) is sufficient for the in vitro experiments.

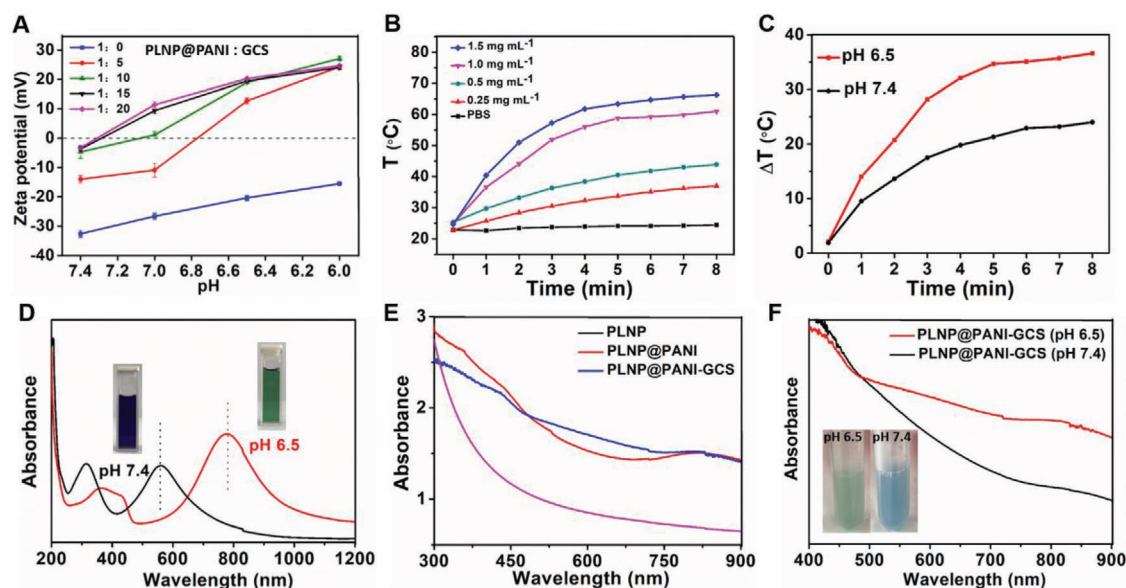


Figure 2. Characterization of PLNP@PANI-GCS: A) pH-dependent zeta potential of the PLNP@PANI-GCS modified with various weight ratios of PLNP@PANI:GCS. B) Photothermal performance of PLNP@PANI-GCS at various concentrations (as PLNPs, pH 6.5) under 808 nm laser irradiation (1.5 W cm^{-2}). C) Changes of increased temperature with irradiation time for PLNP@PANI-GCS (1 mg mL^{-1} as PLNPs) under 808 nm laser irradiation (1.5 W cm^{-2}) at pH 6.5 and pH 7.4. D) UV-vis-NIR absorbance spectra of pure PANI at pH 6.5 and pH 7.4. E) UV-vis-NIR spectra of PLNP, PLNP@PANI, PLNP@PANI-GCS in PBS solution (1 mg mL^{-1} as PLNPs, pH 6.5). F) UV-vis-NIR absorbance spectra of PLNP@PANI-GCS at pH 6.5 and pH 7.4 (1.0 mg mL^{-1} as PLNP).

The photothermal efficiency of PLNP@PANI-GCS is pH dependent. The temperature of PLNP@PANI-GCS (1.0 mg mL^{-1} as PLNP) at pH 6.5 is $12.6 \text{ }^\circ\text{C}$ higher than that at pH 7.4 after 8-min irradiation with 808 nm laser (Figure 2C; Figure S8B, Supporting Information). This result originated from the absorption near 800 nm of the PANI at pH 6.5 (Figure 2D). With the PANI modification, PLNP@PANI and PLNP@PANI-GCS solution (1 mg mL^{-1} as PLNPs) exhibited higher NIR absorbance compared with original PLNPs (1 mg mL^{-1}) at pH 6.5 (Figure 2E). However, the absorbance peaks of PANI were blue-shifted with distinct color change from emerald green at pH 6.5 to deep blue at pH 7.4 due to charge transfer between quinoid and benzenoid rings of PANI (Figure 2D),^[15] causing stronger NIR absorbance at pH 6.5 than pH 7.4 and finally reducing the photothermal conversion capability of PLNP@PANI-GCS from NIR light into heat at pH 7.4 (Figure 2C,F). Besides, the photothermal effect of PLNP@PANI-GCS was stable during the three laser on/off cycles (Figure S8C, Supporting Information). The above results show that PLNP@PANI-GCS under NIR laser irradiation enables to give uninjurious photothermal property in normal physiological environment but to produce hyperthermic effect for killing bacteria in bacterial infection acid microenvironment.

2.3. In Vitro Interactions between PLNP@PANI-GCS and Bacteria/Normal Cells

Escherichia coli (*E. coli*), *Staphylococcus aureus* (*S. aureus*), and MRSA were utilized as a representative of the Gram-negative bacteria, Gram-positive bacteria, and drug-resistance bacteria, respectively, to estimate the antibacterial performance of

PLNP@PANI-GCS. Zeta potential measurements show that the bacteria were negatively charged because of the high contents of anionic phospholipids on the cell walls (Figure 3A). In contrast, PLNP@PANI-GCS was positively charged in acidic environment (pH 6.5). The PLNP@PANI-GCS/bacteria composite was positively charged because the bacteria were encapsulated by the PLNP@PANI-GCS owing to the strong electrostatic interactions at pH 6.5.

The interaction between normal cells and PLNP@PANI-GCS was also examined. 3T3 cells were incubated with PLNP@PANI-GCS in PBS solution either at pH 6.5 or 7.4 for 30 min, the incubated cells were then washed with the corresponding PBS buffer and observed on the laser confocal scanning microscope (LCSM). Figure 3B shows the LCSM images of the incubated cells. The incubation at pH 6.5 led to significant luminescence on the cells because of the electrostatic interaction between negatively charged cells and positively charged PLNP@PANI-GCS (Figure 2A, green line). However, incubation at pH 7.4 gave weak luminescence on the cells because PLNP@PANI-GCS with negative charge at pH 7.4 could not adhere to the negatively charged cells. The above results show that PLNP@PANI-GCS possess strong affinity to bacteria in the acidic environment (pH 6.5) but little affinity to neighboring normal host cells (pH 7.4).

2.4. In Vitro Antimicrobial Activity of PLNP@PANI-GCS

We then evaluated the antibacterial efficiency of PLNP@PANI-GCS. Bacterial survival experiments of *E. coli*, *S. aureus*, and MRSA were carried out in PBS solution (pH 6.5). The results are shown in Figure 4. Compared with the no treatment control

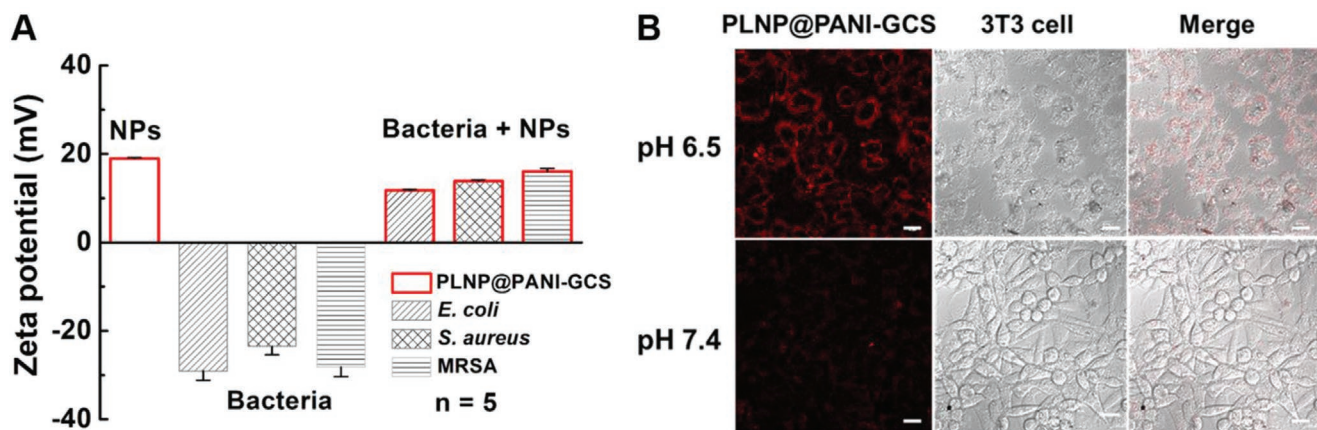


Figure 3. A) Zeta potentials of the bacteria before and after incubation with PLNP@PANI-GCS (1 mg mL^{-1} as PLNPs) at pH 6.5. B) LCSM images of 3T3 cells incubated with PLNP@PANI-GCS (1 mg mL^{-1} as PLNPs) at pH 6.5 and pH 7.4. Scale bar is $20 \mu\text{m}$.

group, the bacteria without 808 nm laser irradiation exhibited negligible bacterial death regardless of the concentration of PLNP@PANI-GCS. Besides, 808 nm laser irradiation only has no killing effect on three kinds of bacteria. However, the bacteria survival rate under 808 nm laser irradiation fell drastically as the concentration of PLNP@PANI-GCS increased. The

use of PLNP@PANI-GCS (1 mg mL^{-1} as PLNPs) in combination with NIR laser irradiation (808 nm , 1.5 W cm^{-2}) killed over 99% of the three kinds of bacteria.

The antibacterial efficiency of PLNP@PANI-GCS and the interaction between PLNP@PANI-GCS and bacteria were also observed intuitively on LCSM. The results are shown in

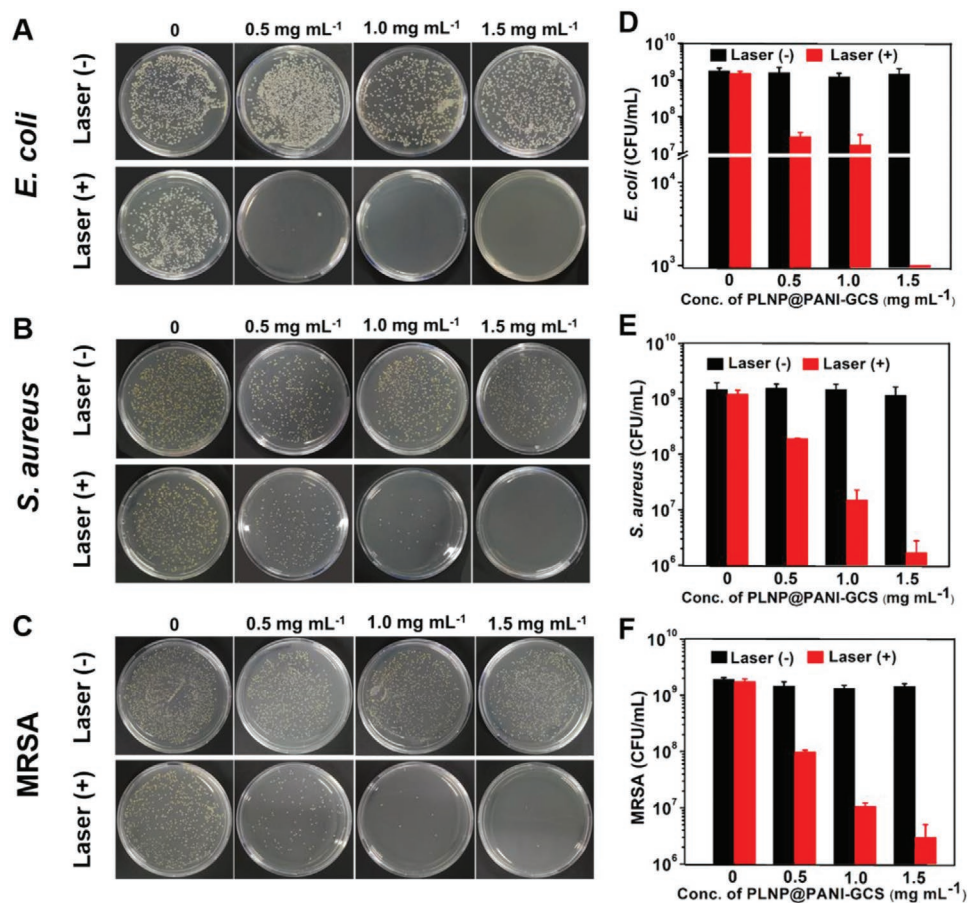


Figure 4. Photographs of bacterial colonies (10^5 times dilution) treated with different concentrations of PLNP@PANI-GCS in vitro (pH 6.5) either with 808 nm laser irradiation or not: A) *E. coli*, B) *S. aureus*, C) MRSA. Viability quantitative results for A, B, and C, respectively: D) *E. coli*, E) *S. aureus*, and F) MRSA. Results are presented as mean \pm SD ($n \geq 3$).

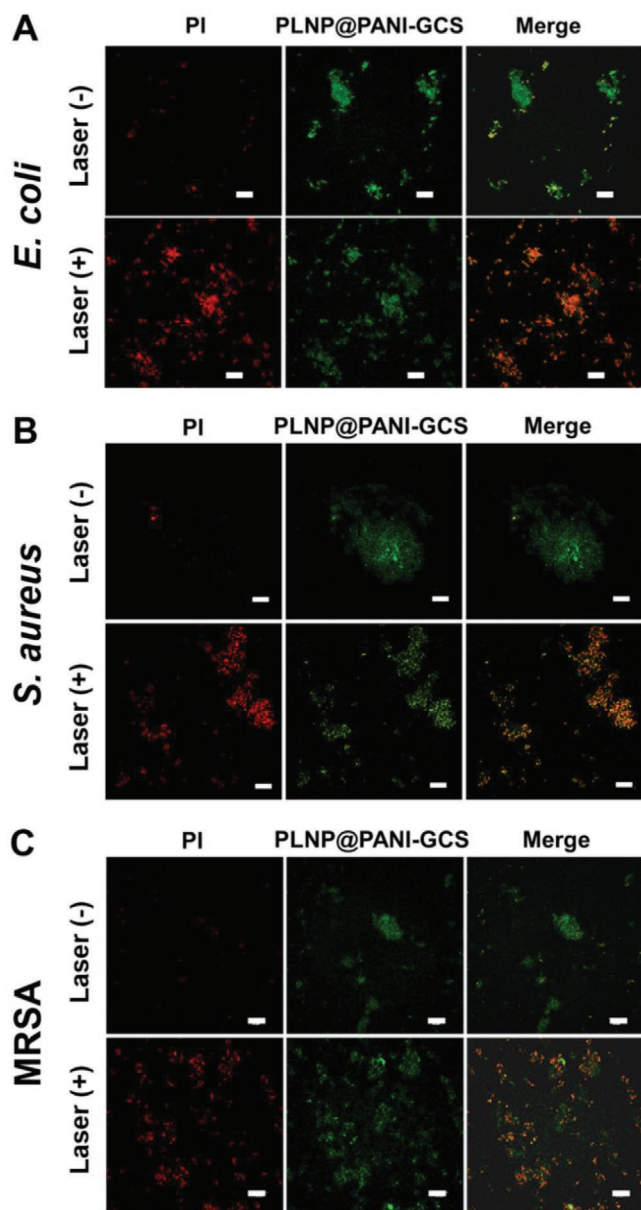


Figure 5. Representative LCSM images for PI stained bacteria: A) *E. coli*, B) *S. aureus*, C) MRSA. The bacteria were incubated with PLNP@PANI-GCS (1 mg mL^{-1} as PLNPs, pH 6.5) with or without 808 nm laser irradiation. Scale bar is 20 μm .

Figure 5 and Figure S9, Supporting Information. Propidium iodide (PI) was added to specifically stain damaged or dead bacteria. The red fluorescence of PI is indicative of dead bacteria, and the green fluorescence is the pseudo color of the luminescence of PLNP@PANI-GCS. The bacteria in the control group (no treatment) show weak red fluorescence whether with laser irradiation or not, indicating few of bacteria dead (Figure S9, Supporting Information). Meanwhile, the bacteria incubated with PLNP@PANI-GCS but without laser irradiation also exhibited weak red fluorescence, suggesting the weak bacteria killing ability of PLNP@PANI-GCS in the absence of laser irradiation (Figure 5). However, the combination of PLNP@PANI-GCS with 808 nm laser irradiation group led to obvious red

fluorescence on the bacteria, indicating a great number of bacteria were killed by the hyperthermia of PLNP@PANI-GCS under laser irradiation. Moreover, the obvious luminescence of PLNP@PANI-GCS on the bacteria confirms that PLNP@PANI-GCS possessed the ability to bond to the bacteria in the acidic environment. The above results show that the photothermal effect and bacteria-targeted imaging capability of PLNP@PANI-GCS makes it promising for the elimination of bacteria.

2.5. In Vitro and In Vivo Safety Tests

The cytotoxicity was primarily evaluated via the MTT assay. The cell viabilities of 3T3 and HepG2 cells all remained over 85% even at the highest dose tested ($600 \mu\text{g mL}^{-1}$ as PLNPs), showing low cytotoxicity of PLNP@PANI-GCS for the multiple cell lines (Figure S10A, Supporting Information). Then, 3T3 cells (as a representative of normal cells) were incubated with PLNP@PANI-GCS at pH 6.5 and 7.4 with or without laser irradiation (Figure S10B, Supporting Information). The cell viabilities of 3T3 cells remained nearly 80% as the concentration of PLNP@PANI-GCS increased to 1 mg mL^{-1} (the dose used in bacteria killing experiment) at pH 7.4 with 8-min laser irradiation. In contrast, the cell viability decreased with the increase of PLNP@PANI-GCS concentration at pH 6.5 under 8-min laser irradiation. The killing efficacy reached nearly 55% when the concentration of PLNP@PANI-GCS reached 1 mg mL^{-1} (as PLNP). Furthermore, in vivo toxicity of PLNP@PANI-GCS was evaluated via histological studies of main organs (heart, liver, spleen, lung, and kidney). All of the examined organs show no obvious lesion or inflammation at 6 days after PLNP@PANI-GCS injection (Figure S10C, Supporting Information). The mice in the PLNP@PANI-GCS treated group showed no death and insignificant body weight drop compared to untreated controls (Figure S11, Supporting Information). All the above results demonstrate that the PLNP@PANI-GCS is an effective photothermal agent for in vivo bacterial elimination without obvious side effect.

2.6. In Vivo Persistent luminescence Imaging of Bacterial Infection

The performance of PLNP@PANI-GCS for in vivo targeting and imaging bacterial infections was evaluated with MRSA infected mice. PLNP, PLNP@PANI, and PLNP@PANI-GCS were intravenously injected into subcutaneous abscess mice, respectively. Two-minute LED light illumination was performed before obtaining the NIR afterglow photographs at the designated time points. The treatment schedule of PLNP@PANI-GCS was illuminated in Figure 6A. As shown in Figure 6B, the mice injected with PLNP@PANI-GCS showed a time-dependent luminescence accumulation in the abscess area, allowing clear NIR afterglow imaging of bacterial infection in vivo. Luminescence in the abscess area appeared at 12 h after PLNP@PANI-GCS injection, and became significant at 24 h to 3 days. However, as the inflammation gradually healed after photothermal therapy, luminescence was reduced and hardly observed at days 5 and 6. In contrast, it is hard to see

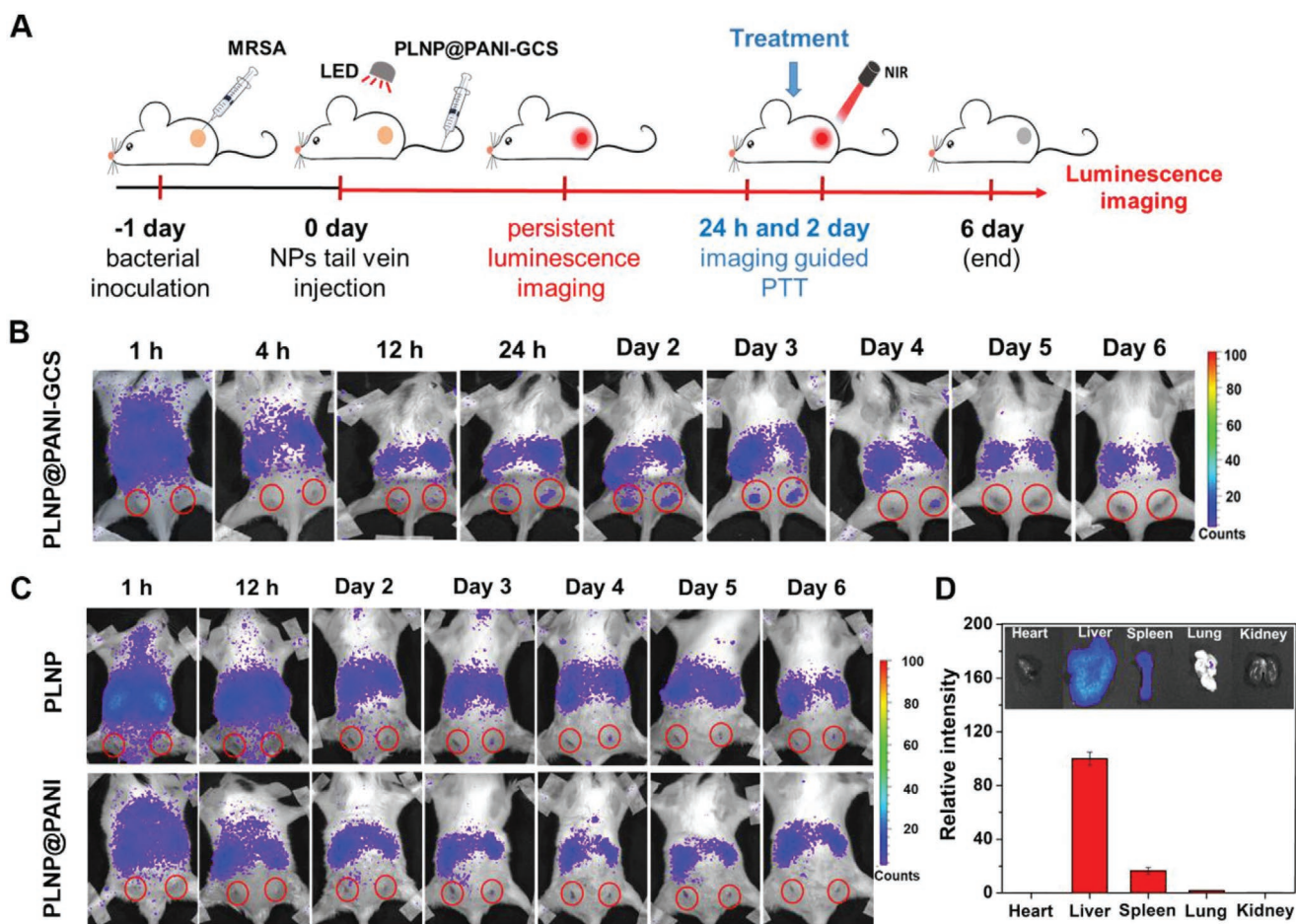


Figure 6. A) Treatment schedule for persistent luminescence imaging-guided PTT in mice, including bacterial inoculation and treatments before harvest. Time-dependent *in vivo* persistent luminescence images for subcutaneous abscess mice model after intravenous injection (2 min illumination with a 650 nm LED light before each acquisition). B) PLNP@PANI-GCS. C) PLNPs and PLNP@PANI. D) Ex vivo persistent luminescence images and relative luminescence intensity of major organs dissected from mice on day 6 after PLNP@PANI-GCS injection. The luminescence intensity of liver organ was set as control. Data were calculated as mean \pm SD.

luminescence signal in the abscess region of the mice in the PLNPs and PLNP@PANI group at all time points (Figure 6C).

Obvious luminescence signal appeared in the spleen and liver due to the strong phagocytosis of reticuloendothelial system. The relative luminescence intensity of isolated organs shows that PLNP@PANI-GCS was mainly accumulated in the liver and spleen, but negligible in other organs (heart, lung and kidney) (Figure 6D; Figure S12, Supporting Information). Moreover, the luminescence signal in the liver and spleen gradually decreased over time, indicating that the PLNP@PANI-GCS could be slowly metabolized by the mice. We then studied the cumulative excretion of the nanoparticles (Figure S13A, Supporting Information). Compared with no treatment group, obvious luminescence signal appeared in the feces of mice injected with PLNP@PANI-GCS in 10 days. The Ga concentration (from PLNP) in the feces determined by ICP-MS shows that 71.5% of the nanoparticles were excreted via feces of mice in 10 days after intravenous injection (Figure S13B, Supporting Information). The long-term retention and imaging of the PLNP@PANI-GCS in the abscess sites provide valuable spatial information for precise PTT.

2.7. In Vivo Photothermal Therapy Ability of PLNP@PANI-GCS

The MRSA-infected mice were randomly divided into four treatment groups (PBS/laser irradiation, PLNP@PANI-GCS, PLNP@PANI-GCS/laser irradiation, and blank control group) to evaluate the *in vivo* PTT performance of PLNP@PANI-GCS. Figure 7A shows the thermal images of the mice in PLNP@PANI-GCS/laser irradiation group and PBS/laser irradiation group. The temperature in the abscess area of mice in PLNP@PANI-GCS/laser irradiation group rapidly increased and reached 52.2 °C under 5-min 808 nm laser irradiation at 24 h post-injection. As shown in Figure 7B, the inflammation and ulceration on the skin of the abscess site disappear and the scars fall off at day 6 for PLNP@PANI-GCS/laser irradiation group, whereas inflammation and obvious abscess necrosis cavity with scab on the skin of the mice remained in PLNP@PANI-GCS group and PBS/laser irradiation group, respectively. To verify the efficacy of infection treatment, the infected muscle tissues were counted using the standard bacterial culture method after 6 days (Figure 7C). Almost no colonies were seen in PLNP@PANI-GCS/laser irradiation group. Compared to the PBS/laser irradiation group and PLNP@PANI-GCS group, the quantitative bacterial

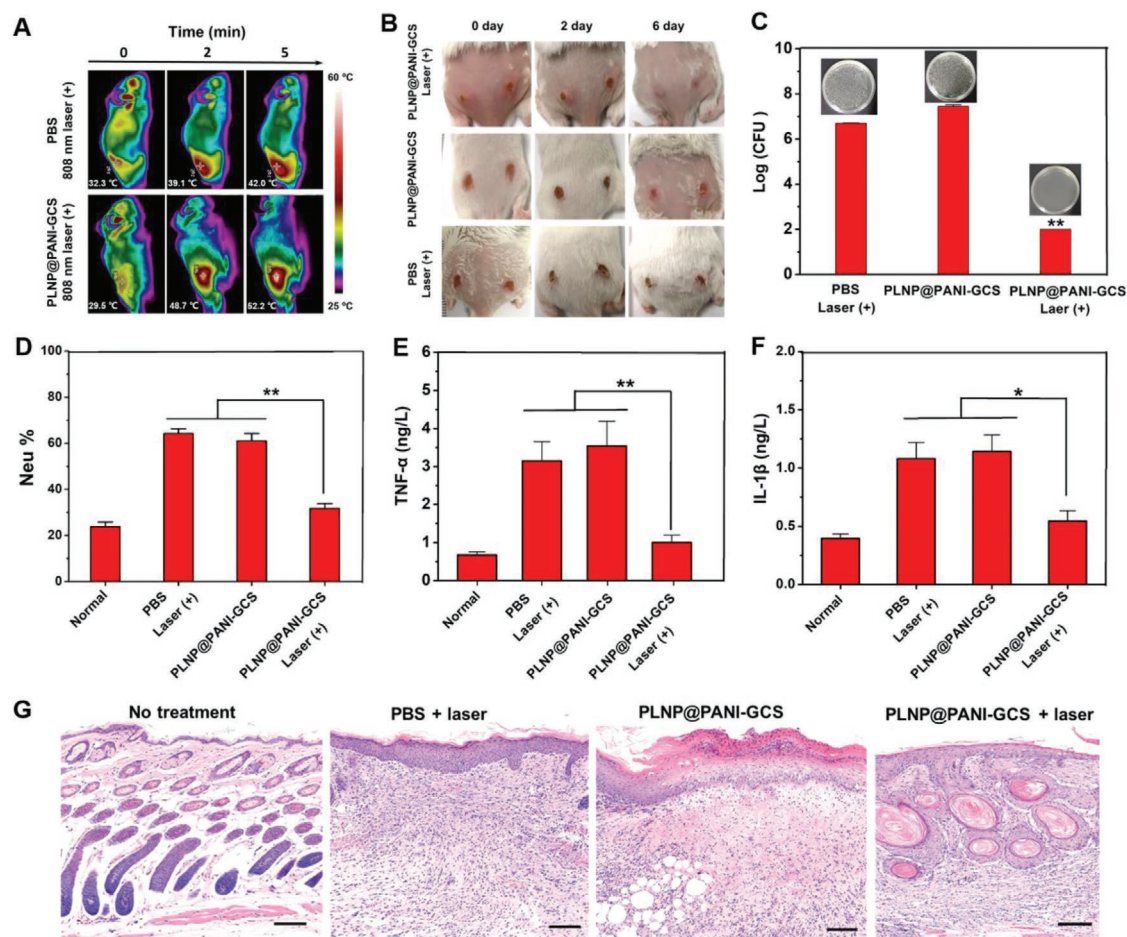


Figure 7. A) Representative thermal images of subcutaneous abscess mice exposed to 808 nm laser (1.5 W cm^{-2}) for different periods after 24 h post injection of PLNP@PANI-GCS. B) Representative photographs of the infectious site of mice after various treatments for 6 days. C) Photograph and related quantitative results of bacterial cultures from the tissues of MRSA infected mice on day 6 after treatment. D) Neutrophil percentage in the blood of mice after various treatments for 6 days. E) Serum TNF- α and F) IL-1 β level of MRSA-infected mice on day 6 after treatment. G) Histological analysis of skin tissues from the abscess sites with different treatments after 6 days. Scale bar is 100 μm . ** denotes extremely significant difference ($p < 0.01$), * denotes significant difference ($p < 0.05$).

colonies were significantly reduced in mice treated with PLNP@PANI-GCS and laser irradiation, indicating great recovery from infection.

The blood neutrophilic granulocyte percentage and serum TNF- α and IL-1 β levels were dramatically lower in PLNP@PANI-GCS/laser irradiation group than the other two groups but no statistical difference from the healthy mice (Figure 7D-F), verifying great recovery of the infected mice in PLNP@PANI-GCS/laser irradiation group. Moreover, hematoxylin and eosin (H&E) staining of the abscess skin tissue was also performed after 6 days (Figure 7G). The skin of the mice in PBS/laser irradiation group and PLNP@PANI-GCS group suffered from massive inflammatory cell infiltration, local skin necrosis, and neutrophil accumulation. In contrast, the PLNP@PANI-GCS/laser irradiation group exhibited less severe inflammatory cell infiltration, and more new capillaries and hair follicles of the mice than the other two groups. The above results imply that PLNP@PANI-GCS with laser irradiation possesses effective antibacterial activity to MDR bacterial infection, and accelerates the healing of infected site.

3. Conclusion

In conclusion, we have reported a core-shell nanostructured PLNP@PANI-GCS for autofluorescence-free persistent luminescence imaging-guided precise photothermal therapy of bacterial infection. The developed PLNP@PANI-GCS nanoplatform integrates the merits of the red LED light-renewable long persistent luminescence, pH-dependent light-heat conversion property, and pH responsive surface charge transition, ensuring the spatial accuracy of the 808 nm laser irradiation and specific heating directly to bacteria. This nanoplatform exhibits specific PTT to acidic bacterial-infected region but no damage to normal tissues. Importantly, the PLNP@PANI-GCS nanoplatform contains no antibiotics, and has great potential in treating multidrug-resistant bacteria infection without the problem of microbial drug resistance. Considering the differences in the microenvironment between bacteria infected region and normal tissue, we believe that the activated photothermal strategy enables further development of more intelligent platforms for targeted bacteria killing.

4. Experimental Section

Synthesis of PLNPs: The NIR-emitting $Zn_{1.2}Ga_{1.6}Ge_{0.2}O_4: Cr^{3+}$ was synthesized via a previous solvothermal approach with minor modification.^[24] Briefly, 1.2 mmol of Zn^{2+} , 1.6 mmol of Ga^{3+} , 0.2 mmol of Ge^{4+} , and 0.0075 mmol of Cr^{3+} were mixed under vigorous stirring, the mixture was then adjusted to pH 8.5 with ammonia solution (28%). The resulting turbid solution was vigorously stirred at room temperature for 3 h, and further heated at 220 °C for 6 h in Teflon-lined autoclave. After cooling to room temperature, the mixture was centrifuged and washed with ultrapure water and ethanol for three times, then dried in a vacuum for 12 h. The obtained powder was sintered at 800 °C in air for 1 h, dispersed in ultrapure water, and centrifuged at 2500 rpm for 5 min to obtain PLNPs in supernatant.

Preparation of PLNP@PANI-GCS Nanocomposites: PLNP@PANI was synthesized via an in situ chemical oxidative polymerization with modification.^[14a,25] PLNP (125 mg) was added into the mixture solution of aniline (20 mmol L⁻¹ in 0.1 mol L⁻¹ HCl, 27 mL), 3-aminobenzoic acid (aniline-COOH aqueous solution, 20 mmol L⁻¹, 3 mL), SDS (400 mmol L⁻¹, 6 mL). The solution was sonicated for 60 s, and kept magnetically stirring for 2 h. APS (20 mmol L⁻¹ in 10 mmol L⁻¹ HCl, 30 mL) was then injected into the mixture to induce the polymerization reaction. The final solution was stirred at room temperature for 12 h to complete the polymerization. The mixture was centrifuged at 10 000 rpm for 15 min and washed with ultrapure water and HCl to remove excess reactants. Thus, the nanocomposites with PLNPs core and PANI shell (PLNP@PANI) with -COOH groups on their surface were obtained.

PLNP@PANI-GCS was further synthesized via an amidation reaction between PLNP@PANI and GCS. Briefly, PLNP@PANI (5 mg as PLNP) was dissolved in 5 mL of 10 mmol L⁻¹ PBS (pH 6.0), to which EDC (15 mg) and NHS (45 mg) were added and preactivated for 2 h. GCS (50 mg) was sequentially added into the mixture under quick stirring and the pH was adjusted to 8.0 with NaOH solution (1 mol L⁻¹) for another 12 h reaction at room temperature. The resulting PLNP@PANI-GCS was collected, washed with PBS and ultrapure water, redispersed in PBS, and kept at 4 °C for further use.

Photothermal Test of PLNP@PANI-GCS: PLNP@PANI-GCS was dispersed in PBS (10 mmol L⁻¹, pH 6.5, and pH 7.4) at various concentrations (0, 0.25, 0.5, 1.0, 1.5 mg mL⁻¹, calculated as PLNPs), then 1 mL of the solution was irradiated with an NIR laser (808 nm, 1.5 W cm⁻²) in a centrifuge tube for 8 min (1 mL PBS was used as control). During irradiation, the temperature variation was monitored by an FLIR thermal camera.

Preparation of Bacterial Cultures: *E. coli*, *S. aureus*, and MRSA were used as the model organism to evaluate the photothermal antibacterial efficiency of PLNP@PANI-GCS. Bacteria were cultured in 5 mL Luria Bertani broth medium with shaking (180 rpm) at 37 °C for 12 h. The bacteria on the exponential phase were separated and resuspended in 1 mL PBS (pH 6.5) next day.

In Vitro Interaction of PLNP@PANI-GCS and Bacteria: The in vitro interaction between PLNP@PANI-GCS and the model bacteria in the acidic environment was evaluated at pH 6.5. One milliliter mixed solution of bacteria ($\approx 10^9$ colony forming units (CFU) mL⁻¹) and PLNP@PANI-GCS (1 mg mL⁻¹ as PLNPs in final mixed solution) was incubated at 37 °C for 30 min. The free PLNP@PANI-GCS was then removed by centrifugation and the bottom pellet (PLNP@PANI-GCS/bacteria composite) was resuspended in 1 mL PBS (pH 6.5) to measure its zeta potential. For comparison, the zeta potentials of the modal bacteria and PLNPs@PANI-GCS were also measured under the same conditions, respectively.

In Vitro Photothermal Ablation of Bacteria: Five hundred microliters of three strains (*E. coli*, *S. aureus*, and MRSA) in PBS at pH 6.5 ($\approx 10^9$ CFU mL⁻¹ in final mixed solution) were mixed with 500 μ L of PLNPs@PANI-GCS solution in centrifuge tube to reach the final concentrations of 0.5, 1.0, and 1.5 mg mL⁻¹ (as PLNPs) for 30-min incubation at 37 °C. Then, the photothermal ablation of the bacteria was tested on four groups: (1) bacteria in PBS without laser irradiation (control group), (2) bacteria in PBS under laser irradiation, (3) the incubated bacteria and

PLNP@PANI-GCS in PBS without laser irradiation, (4) the incubated bacteria and PLNP@PANI-GCS in PBS under laser irradiation. Laser irradiation was performed with an NIR laser (808 nm, 1.5 W cm⁻²) for 8 min. 100 μ L of bacterial suspension was taken from each group and gradually diluted 10⁶ times. Thereafter, 100 μ L of the each diluted solutions was spread evenly onto the Luria Bertani broth plates. After culturing in an aerophilic environment at 37 °C for 20 to 24 h, the colonies number was counted.

Bacterial Staining and Confocal Imaging: The bacteria cells in the above four groups were respectively stained by incubating with 10 μ g mL⁻¹ PI in dark for 15 min. After incubation, the hybrid of bacteria were centrifuged, washed with PBS buffer, and resuspended in PBS at pH 6.5. 10 μ L of bacterial solution was dropped onto a glass slide. The glass slide was covered with a coverslip for LCSM characterization of the live and dead bacteria cells. The 561 and 640 nm laser was set to excite the PI and PLNP@PANI-GCS, respectively.

In Vitro Interaction of PLNPs@PANI-GCS and Normal Cells: 3T3 cells were cultured in DMEM medium with 10% FBS and 1% antibiotics (penicillin-streptomycin) in a humidified atmosphere containing 5% CO₂ at 37 °C. 1×10^5 cells were seeded in confocal cuvette to adhere for 24 h, and then incubated with PLNP@PANI-GCS (1 mg mL⁻¹ as PLNPs in DMEM, 1 mL) at pH 6.5 and 7.4, respectively. After 30 min incubation, the cells were washed with corresponding PBS solution and resuspended in DMEM medium to acquire luminescence images on LCSM.

In Vitro Cytotoxicity Assay: MTT assays were carried out to estimate the cytotoxicity of PLNP@PANI-GCS. 3T3 and HepG2 cells were cultured in DMEM medium with 10% FBS and 1% antibiotics at 37 °C under a 5% humidified atmosphere. Briefly, 3T3 and HepG2 cells were separately cultured in a 96-well plate at a density of 1×10^4 cells per well (100 μ L DMEM medium/well). After cultivation overnight, the old DMEM medium was replaced with the fresh DMEM medium containing different concentrations of PLNP@PANI-GCS for another 24-h incubation. The cells incubated without PLNP@PANI-GCS were used as blank control. In MTT assay of PLNP@PANI-GCS under 808 nm laser on 3T3 cells, 3T3 cells were incubated with different concentrations of PLNP@PANI-GCS at pH 6.5 and pH 7.4 for 30 min, respectively. Then, the old DMEM medium containing PLNP@PANI-GCS was replaced with the fresh DMEM medium to remove the uncombined PLNP@PANI-GCS and 8 min irradiation with 808 nm laser was applied to the cells. Then, the cells were washed with PBS completely and incubated in 100 μ L of culture medium containing MTT (0.5 mg mL⁻¹) at 37 °C for additional 4 h. After the supernatants were removed, 100 μ L DMSO was carefully added into each well. The plate was softly shaken for 10 min and then the absorbance at 490 nm was measured on a microplate reader.

Murine Infection Model: Female Balb/c mice (3–4 weeks) were purchased from Shanghai Slac Laboratory Animal Co. Ltd (Shanghai, China). All animal experiments were in compliant with the Jiangnan University of Use and Care of Laboratory Animals, and were performed ethically and humanely. The MRSA infected mouse model was built to evaluate in vivo luminescence imaging and PTT effect of PLNP@PANI-GCS. To produce subcutaneous abscesses, 100 μ L of MRSA (about 10⁷ CFU mL⁻¹) in PBS buffer was subcutaneously injected into the shaved and disinfected back of anesthetized mice. After 24 h, a subcutaneous abscess was observed on the infected site.

In Vivo Luminescence Imaging of MRSA-Infected Subcutaneous Abscesses: PLNP, PLNP@PANI, and PLNP@PANI-GCS (150 μ L, 4 mg mL⁻¹ as PLNP) were intravenously injected into anesthetized subcutaneous abscess mice, respectively. The luminescence distribution of the implanted PLNP@PANI-GCS NPs was monitored at specified time points (1 h, 4 h, 12 h, 24 h, 2 d, 3 d, 4 d, 5 d and 6 d) on an in vivo IVIS imaging system. The distribution of the luminescence of PLNP and PLNP@PANI was monitored for comparison. Before acquiring luminescence images, the mice was excited with a 650 nm LED light (5000 lm) for 2 min.

In Vivo Photothermal Antibacterial Therapy: After 24-h MRSA infection, the mice were treated with antibacterial therapy. The mice (n = 5) were randomly divided into four groups: group I (PBS/laser irradiation), group II (PLNP@PANI-GCS), group III (PLNP@PANI-GCS/laser irradiation), and group IV (healthy mice without any treatment, blank control group).

PLNP@PANI-GCS (150 μL , 4 mg mL^{-1} as PLNPs) were intravenously injected into the mice of group II and group III. Five-minute irradiation (808 nm laser, 1.5 W cm^{-2}) was applied to the subcutaneous abscess of group I and group III at 24 h and 2 d. The thermographic images in abscess were recorded on an IR thermal camera at 24 h. The body weight of mice was measured every day. All mice were sacrificed after 6-d treatment, and the skin tissues and major organs (heart, liver, lung, kidney, and spleen) were fixed in a 4% formaldehyde solution for H&E staining.

Blood Biochemical Analysis: Blood was extracted from the mice in the four groups studied after 6-d treatment. The neutrophilic granulocyte percentage was measured by automatic hemocyte analyzer (BC-5000Vet, ThermoFisher, USA). TNF- α and IL-1 β in the serum of mice blood were determined by the ELISA kits.

Supporting Information

Supporting Information is available from the Wiley Online Library or from the author.

Acknowledgements

The authors appreciate the financial support from the National Natural Science Foundation of China (No. 21934002, 21804056, and 21804057), the China Postdoctoral Science Foundation (No. 2018M630511 and 2018M630509), the Postdoctoral Innovative Talent Support Program (No. BX20180130), and the Natural Science Foundation of Jiangsu Province, China (No. BK20180581 and BK20180584), the National First-class Discipline Program of Food Science and Technology (No. JUFSTR20180301), the Fundamental Research Funds for the Central Universities (No. JUSR51714B and JUSR11846), and Collaborative Innovation Center of Food Safety and Quality Control in Jiangsu Province.

Conflict of Interest

The authors declare no conflict of interest.

Keywords

bacterial infection, charge conversion, imaging-guided photothermal therapy, persistent luminescence nanoparticles

Received: October 31, 2019

Revised: January 13, 2020

Published online:

- [1] a) K. E. Jones, N. G. Patel, M. A. Levy, A. Storeygard, D. Balk, J. L. Gittleman, P. Daszak, *Nature* **2008**, 451, 990; b) K. Vasilev, V. Sah, K. Anselme, C. Ndi, M. Mateescu, B. Dollmann, P. Martinek, H. Ys, L. Ploux, H. J. Griesser, *Nano Lett.* **2010**, 10, 202; c) J. Huang, J. Zhou, J. Zhuang, H. Gao, D. Huang, L. Wang, W. Wu, Q. Li, D. P. Yang, M. Y. Han, *ACS Appl. Mater. Interfaces* **2017**, 9, 36606.
- [2] a) M. Rai, A. P. Ingle, R. Pandit, P. Paralikar, I. Gupta, M. V. Chaud, C. A. Santos, *Int. J. Pharm.* **2017**, 532, 139; b) C. Willyard, *Nature* **2017**, 543, 15.
- [3] E. D. Brown, G. D. Wright, *Nature* **2016**, 529, 336.
- [4] a) J. H. Kim, C. H. Jeong, W. J. Kim, *Adv. Drug Deliv. Rev.* **2016**, 98, 99; b) H. Lin, Y. Wang, S. Gao, Y. Chen, J. Shi, *Adv. Mater.* **2018**, 30, 1703284; c) H. Lin, S. Gao, C. Dai, Y. Chen, J. Shi, *J. Am. Chem.*

- Soc.* **2017**, 139, 16235; d) J. Shao, C. Ruan, H. Xie, Z. Li, H. Wang, P. Chu, X. F. Yu, *Adv. Sci.* **2018**, 5, 1700848.
- [5] a) E. S. Day, J. G. Morton, J. L. West, *J. Biomech. Eng.* **2009**, 131, 074001; b) Z. H. Bao, X. R. Liu, Y. D. Liu, H. Z. Liu, K. Zhao, *Asian J. Pharm. Sci.* **2016**, 11, 349.
- [6] a) L. D. Kong, L. X. Xing, B. Q. Zhou, L. F. Du, X. Y. Shi, *ACS Appl. Mater. Interfaces* **2017**, 9, 15995; b) L. Cheng, J. J. Liu, X. Gu, H. Gong, X. Z. Shi, T. Liu, C. Wang, X. Y. Wang, G. Liu, H. Y. Xing, W. B. Bu, B. Q. Sun, Z. Liu, *Adv. Mater.* **2014**, 26, 1886; c) X. D. Song, W. T. Shang, L. Peng, H. M. Jiang, K. Wang, C. H. Fang, J. Tian, *Nanomedicine* **2018**, 13, 1681.
- [7] G. S. Hong, S. O. Diao, A. L. Antaris, H. J. Dai, *Chem. Rev.* **2015**, 115, 10816.
- [8] X. Huang, S. Tang, X. Mu, Y. Dai, G. Chen, Z. Zhou, F. Ruan, Z. Yang, N. Zheng, *Nat. Nanotechnol.* **2011**, 6, 28.
- [9] a) Y. Ju, H. Zhang, J. Yu, S. Tong, N. Tian, Z. Wang, X. Wang, X. Su, X. Chu, J. Lin, Y. Ding, G. Li, F. Sheng, Y. Hou, *ACS Nano* **2017**, 11, 9239; b) J. Li, F. Jiang, B. Yang, X. R. Song, Y. Liu, H. H. Yang, D. R. Cao, W. R. Shi, G. N. Chen, *Sci. Rep.* **2013**, 3, 1998.
- [10] a) Y. Ju, B. Dong, J. Yu, Y. Hou, *Nano Today* **2019**, 26, 108; b) H. S. Jung, P. Verwilt, A. Sharma, J. Shin, J. L. Sessler, J. S. Kim, *Chem. Soc. Rev.* **2018**, 47, 2280.
- [11] a) Y. D. Zhu, S. P. Chen, H. Zhao, Y. Yang, X. Q. Chen, J. Sun, H. S. Fan, X. D. Zhang, *ACS Appl. Mater. Interfaces* **2016**, 8, 34209; b) H. Zhang, L. Xiong, X. Liao, K. Huang, *Macromol. Rapid Commun.* **2016**, 37, 149.
- [12] a) Z. Wang, Y. Ju, Z. Ali, H. Yin, F. Sheng, J. Lin, B. Wang, Y. Hou, *Nat. Commun.* **2019**, 10, 4418; b) S. Luo, X. Tan, S. Fang, Y. Wang, T. Liu, X. Wang, Y. Yuan, H. Sun, Q. Qi, C. Shi, *Adv. Funct. Mater.* **2016**, 26, 2826.
- [13] a) Q. Zhou, M. Abbas, L. Zhao, S. Li, G. Shen, X. Yan, *J. Am. Chem. Soc.* **2017**, 139, 1921; b) B. Guo, G. Feng, P. N. Manghnani, X. Cai, J. Liu, W. Wu, S. Xu, X. Cheng, C. Teh, B. Liu, *Small* **2016**, 12, 6243.
- [14] a) E. Ju, K. Dong, Z. Liu, F. Pu, J. Ren, X. Qu, *Adv. Funct. Mater.* **2015**, 25, 1574; b) W. Qian, C. Yan, D. He, X. Yu, L. Yuan, M. Liu, G. Luo, J. Deng, *Acta Biomater.* **2018**, 69, 256; c) J. Wang, R. Yan, F. Guo, M. Yu, F. Tan, N. Li, *Nanotechnology* **2016**, 27, 285102; d) Y. Wang, Y. Xiao, R. Tang, *Chem. Eur. J.* **2014**, 20, 11826; e) C. Wang, H. Xu, C. Liang, Y. Liu, Z. Li, G. Yang, L. Cheng, Y. Li, Z. Liu, *ACS Nano* **2013**, 7, 6782.
- [15] a) Z. A. I. Mazrad, C. A. Choi, S. H. Kim, G. Lee, S. Lee, I. In, K. D. Lee, S. Y. Park, *J. Mater. Chem. B* **2017**, 5, 7099; b) J. Zhou, Z. Lu, X. Zhu, X. Wang, Y. Liao, Z. Ma, F. Li, *Biomaterials* **2013**, 34, 9584; c) J. Yang, J. Choi, D. Bang, E. Kim, E. K. Lim, H. Park, J. S. Suh, K. Lee, K. H. Yoo, E. K. Kim, Y. M. Huh, S. Haam, *Angew. Chem. Int. Ed.* **2011**, 50, 441; d) Y. C. Hong, S. Hwang, D. Heo, B. Kim, M. Ku, E. Lee, S. Haam, D. S. Yoon, J. Yang, J. S. Suh, *Nanoscale* **2015**, 7, 1661.
- [16] A. J. Heeger, *Angew. Chem. Int. Ed.* **2001**, 40, 2591.
- [17] a) B. Y. Wu, X. P. Yan, *Chem. Commun.* **2015**, 51, 3903; b) S. K. Sun, H. F. Wang, X. P. Yan, *Acc. Chem. Res.* **2018**, 51, 1131; c) A. Abdulkayum, J. T. Chen, Q. Zhao, X. P. Yan, *J. Am. Chem. Soc.* **2013**, 135, 14125; d) Y. Li, M. Gecevicius, J. Qiu, *Chem. Soc. Rev.* **2016**, 45, 2090; e) S. Q. Wu, C. W. Chi, C. X. Yang, X. P. Yan, *Anal. Chem.* **2016**, 88, 4114.
- [18] a) Z. Li, Y. Zhang, X. Wu, L. Huang, D. Li, W. Fan, G. Han, *J. Am. Chem. Soc.* **2015**, 137, 5304; b) Z. Pan, Y. Y. Lu, F. Liu, *Nat. Mater.* **2012**, 11, 58; c) A. Bessière, S. K. Sharma, N. Basavaraju, K. R. Priolkar, L. Binet, B. Viana, A. J. J. Bos, T. Maldiney, C. Richard, D. Scherman, D. Gourier, *Chem. Mater.* **2014**, 26, 1365; d) Y. Yun, Y. W. Cho, K. Park, *Adv. Drug Deliv. Rev.* **2013**, 65, 822; e) J. Shi, X. Sun, J. Zhu, J. Li, H. Zhang, *Nanoscale* **2016**, 8, 9798.
- [19] a) L. Yan, S. H. Crayton, J. P. Thawani, A. Amirshaghghi, A. Tsourkas, Z. Cheng, *Small* **2015**, 11, 4870; b) K. Nwe, C. H. Huang, A. Tsourkas, *J. Med. Chem.* **2013**, 56, 7862; c) W. Wu,

- S. Y. Lee, X. B. Wu, J. Y. Tyler, H. Wang, Z. Ouyang, K. Park, X. M. Xu, J. X. Cheng, *Biomaterials* **2014**, *35*, 2355; d) S. H. Crayton, A. Tsourkas, *ACS Nano* **2011**, *5*, 9592.
- [20] T. Maldiney, A. Bessiere, J. Seguin, E. Teston, S. K. Sharma, B. Viana, A. J. J. Bos, P. Dorenbos, M. Bessodes, D. Gourier, D. Scherman, C. Richard, *Nat. Mater.* **2014**, *13*, 418.
- [21] B. P. Jiang, L. Zhang, Y. Zhu, X. C. Shen, S. C. Ji, X. Y. Tan, L. Cheng, H. Liang, *J. Mater. Chem. B* **2015**, *3*, 3767.
- [22] C. Korupalli, C. C. Huang, W. C. Lin, W. Y. Pan, P. Y. Lin, W. L. Wan, M. J. Li, Y. Chang, H. W. Sung, *Biomaterials* **2017**, *116*, 1.
- [23] D. O. Lapotko, *Theranostics* **2013**, *3*, 138.
- [24] a) J. Wang, Q. Ma, X. Hu, H. Liu, W. Zheng, X. Chen, Q. Yuan, W. Tan, *ACS Nano* **2017**, *11*, 8010; b) M. Allix, S. Chenu, E. Véron, T. Poumeyrol, E. A. Kouadri-Boudjelthia, S. Alahrache, F. Porcher, D. Massiot, F. Fayon, *Chem. Mater.* **2013**, *25*, 1600; c) L. J. Chen, S. K. Sun, Y. Wang, C. X. Yang, S. Q. Wu, X. P. Yan, *ACS Appl. Mater. Interfaces* **2016**, *8*, 32667.
- [25] a) J. Wang, X. Tan, X. Pang, L. Liu, F. Tan, N. Li, *ACS Appl. Mater. Interfaces* **2016**, *8*, 24331; b) X. Tan, J. Wang, X. Pang, L. Liu, Q. Sun, Q. You, F. Tan, N. Li, *ACS Appl. Mater. Interfaces* **2016**, *8*, 34991.